Available online at www.sciencedirect.com
SCIENCE DIRECT
Journal of the European Ceramic Society 26 (2006) 1351–1362
www.elsevier.com/locate/jeurceramsoc

Effect of $LiAl_5O_8$ additions on the sintering and optical transparency of LiAlON

D. Clay [a], D. Poslusny [a], M. Flinders [a], S.D. Jacobs [b], R.A. Cutler [a,*]

[a] *Ceramatec Inc., 2425 S. 900 W., Salt Lake City, UT 84119, USA*
[b] *University of Rochester, Center for Optical Manufacturing and Laboratory for Laser Energetics, 240 East River Road, Rochester, NY 14623, USA*

Received 27 September 2004; received in revised form 15 January 2005; accepted 28 January 2005
Available online 31 March 2005

Abstract

$LiAl_5O_8$ (zeta alumina) was reaction sintered with α-Al_2O_3 and AlN to produce γ-LiAlON. Zeta alumina transforms from a primitive to a face-centered cubic structure above 1290 °C with a lattice parameter similar to γ-AlON. Weight loss measurements combined with XRD suggest solubility of Li in the spinel structure at elevated temperatures. The Vickers hardness, at a 1-kg load, of the pressureless sintered LiAlON was 16.5 ± 0.5 GPa, independent of the grain size or amount of zeta alumina added, for $LiAl_5O_8$ additions ranging between 0 and 16 wt.%. In-line transmission in the visible and near-IR regions increased with increasing grain size, most likely due to pore coalescence.
© 2005 Elsevier Ltd. All rights reserved.

Keywords: AlON; Sintering; Transparency; LiAlON; $LiAl_5O_8$

1. Introduction

Aluminum oxynitride spinel, known by the acronym AlON, is a solid solution composed of aluminum, oxygen, and nitrogen as a cubic spinel structure.[1] McCauley[2] showed that what has come to be known to many as AlON (i.e., $5AlN{\cdot}9Al_2O_3$) can be modeled with a constant anion model. The spinel cation vacancies decrease as the nitrogen content increases.[2,3] McCauley and Corbin[4] showed that transparent AlON could be fabricated by reaction sintering AlN and Al_2O_3 in the 5:9 molar ratio, as well as mapped out the region for γ-AlON. Later work[5] showed that four different spinel AlON phases exist at molar ratios of approximately 10 mol% AlN (δ-AlON), 17 mol% AlN (ø′-AlON), 21 mol% AlN (γ′-AlON), and 36 mol% AlN (γ-AlON). Gamma AlON exists in the widest stability range, which is a function of temperature,[5–10] with eutectoid decomposition into Al_2O_3 and AlN below about 1640 °C.[7] Stabilization at lower temperatures is possible with Mg additions, but the intrinsic mechanical properties are somewhat compromised.[11,12] As Corbin[5] points out in his review article, AlON has been synthesized below 1000 °C from gaseous reactants. Due to stability issues, including oxidation, AlON is a metastable low-temperature material best suited for use below 500 °C.

AlON has excellent optical properties[13] with useful transmission from about 0.2 μm in the UV through the visible range to about 6.0 μm in the near-IR. While AlON is denser than AlN, its cubic structure allows it to be made transparent, even at considerable thickness, while maintaining decent mechanical properties.[14] AlON, magnesium aluminum spinel, and sapphire are all candidates for transparent armor systems. AlON and $MgAl_2O_4$ have the advantage of easier processing and lower cost than sapphire.[15] Raytheon Company (now Surmet) has used AlON for IR domes for missiles for many years.[16–19]

Relatively expensive powders and high finishing costs prevent the wide-spread use of AlON. The present research investigated the use of inexpensive α-Al_2O_3 as the primary component in the starting powders and hypothesized that

* Corresponding author. Tel.: +1 801 978 2126; fax: +1 801 954 2008.
E-mail address: cutler@ceramatec.com (R.A. Cutler).

0955-2219/$ – see front matter © 2005 Elsevier Ltd. All rights reserved.
doi:10.1016/j.jeurceramsoc.2005.01.056

a sintering additive, such as zeta alumina ($LiAl_5O_8$) with a melting point of 1915 °C,[20] would aid in densification via transient liquid phase sintering. A beneficial side effect of using zeta alumina as a transient liquid phase is that grain growth inhibition may occur.[21] Current AlON is coarse grained and a finer grain size would not only improve strength, but could allow easier polishing due to a reduced tendency for grain pullout.

2. Experimental

2.1. Powder processing

An α-Al_2O_3 powder (Sasol North America grade SPA-0.05) was chosen as the alumina source due to its high purity (Si = 14 ppm, Na = 7 ppm, Fe = 7 ppm, Mg = 6 ppm, and Ca = 4 ppm) and small particle size (d_{50} = 0.47 μm with BET surface area of 7.6 m^2/g). The AlN powder (Tokuyama Soda, grade F) was nine times more expensive, with lower surface area (3.4 m^2/g) but still had low impurities (Fe < 10 ppm and Si = 9 ppm) other than O (0.78%) and C (290 ppm). Polyvinyl pyrrolidone (PVP) with molecular weights of 9700 g/mol (ISP grade K-15) or 66,800 g/mol (ISP grade K-30) disperse both AlN and Al_2O_3 in ethanol (Ashland Chemical grade PM 509). The lower molecular weight PVP is a more effective dispersant as shown in Fig. 1. The Al_2O_3 was dispersed at a solids content of 20 vol.% in ethanol, while the AlN was dispersed at 40 vol.% solids. Based on these results slips were made with the combined at a solids content of 40 vol.% solids in ethanol with 0.5 wt.% K-15 PVP as a dispersant.

Li_2CO_3 (Baker reagent grade 2362-01) and α-Al_2O_3 powders were milled for 24 h in ethanol using Y-TZP media (Tosoh TZ-3Y) in a high-density polyethylene (HDPE) container. Zeta alumina was formed as

$$Li_2CO_3 + 5Al_2O_3 \rightarrow 2LiAl_5O_8 + CO_2\uparrow \quad (1)$$

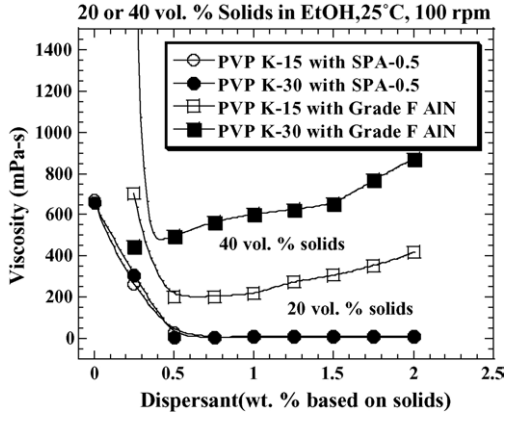

Fig. 1. Effect of dispersant content on slip viscosity. Note that AlN is easily overdispersed. A dispersant level of 0.5 wt.% K-15, based on solids, was used for all processing.

by heating the powder mixture in air to temperatures between 900 and 1500 °C and holding for 2 h. X-ray diffraction was used to confirm the extent of reaction. The calcined zeta alumina was screened −325 mesh (44 μm) and treated like a raw material for batching compositions.

Y_2O_3 (Molycorp grade 5900), BN (GE Advanced Ceramics grade Polartherm 120), MgO (Baker Chromatographic grade), YF_3 (Molycorp), LiF (Cerac grade L-1065), Nb_2O_5 (PIDC grade 99.9%), and Si_3N_4 (Toyo Soda grade TS-7) were all investigated as sintering aids.

High purity Al_2O_3 (AD999 from Union Process) or Y-TZP milling media were used in HDPE or urethane-lined vibratory milling containers. Powder processing was accomplished by dispersing the raw materials in ethanol with PVP and vibratory milling to break down agglomerates and reduce particle size. Typical milling times were 48 h with Y-TZP media. A wide variety of compositions were prepared using vibratory milling, either in the small 250 ml jars or in a larger urethane-lined mill where the batch size was up to 1.5 kg of reactants.

Dried powders were lubed with paraffin, using hexane to dissolve the binder prior to mixing it into the previously milled powders. The amount of paraffin was 2 wt.%, based on the solids content of the dried powder. The slurries were stir-dried and then screened −60 mesh using a nylon sieve. Lubed powders were pressed in a steel die at 35 MPa uniaxially and then isopressed at 170–200 MPa isostatically. Green density was measured after removing the binder by heating in air to 400–600 °C.

2.2. Sintering and characterization

Sintering was carried out in pyrolytic BN crucibles with parts packed in powder. The powder bed was a mixture of 25 wt.% BN and 75 wt.% AlON formed by reacting alumina and aluminum nitride. The typical molar ratio of the AlON packing powder was 30 mol% AlN. The BN helped to keep the AlON powder beds from sintering together. The purpose of the packing powder was to protect the AlON from the graphite in the furnace and to reduce the tendency for the material to volatilize. Sintering temperatures ranged from 1600 to 2000 °C and isothermal holding time ranged from 1 to 15 h. A slight overpressure (0.5 bar) of nitrogen was used for most experiments. Hot isostatic pressing (HIPing) of selected samples was performed at American Isostatic Pressing Inc. (Columbus, OH) using N_2 gas pressurized to 207 MPa at 2000 °C.

Characterization of sintered parts included density measurements, X-ray diffraction, SEM evaluation of fracture surfaces, and Vickers hardness measurements with a 1-kg load. Surface roughness data were obtained on a white light interferometer (Zygo New View 5000) using a 20X objective (except where otherwise indicated) that generated areal data for regions 0.349 mm by 0.262 mm in size. At least five sites on each surface were evaluated to determine averages and standard deviations. Finishing studies were performed in three stages. Deterministic microgrinding (DMG)[22] was

conducted on one side of each of five 25 mm diameter flat samples, each with a different grain size. Starting from an initial peak to valley (p–v) surface roughness of ~20 μm, metal bonded diamond ring tools were used to remove 100 μm (rough grind), 50 μm (medium grind), and ~25 μm (fine grind). Surfaces were then processed with magnetorheolocial finishing (MRF)[23] to evaluate the evolution of surface microroughness. MRF was performed on a QED Technologies Q22Y MRF machine using a standard nanodiamond MR fluid. Uniform removal runs lasting from 2 to 3 h were required to take off 4–7 μm of material from sample surfaces. No attempt was made to achieve or maintain any degree of surface form accuracy. Additional processing was performed on these samples using bound abrasive polishing laps, as described previously.[24] Areas of evaluation were adjusted upward with increasing grain size to assure that sufficient numbers of grains were included in these roughness measurements. Grain size was measured by a linear intercept method. In-line transmission was measured using a spectrometer (Perkin-Elmer Lambda 900) for wavelengths between 3 and 33 μm.

3. Results

Al_2O_3/AlN compositions without sintering aids were made with molar ratios of 2.3, 3.0 and 4.0. The theoretical density of unreacted mixtures range between 3.86 g/cm^3 (30 mol% AlN) and 3.90 g/cm^3 (20 mol% AlN). The idea was to sinter to as high of a density as possible in the AlN/Al_2O_3

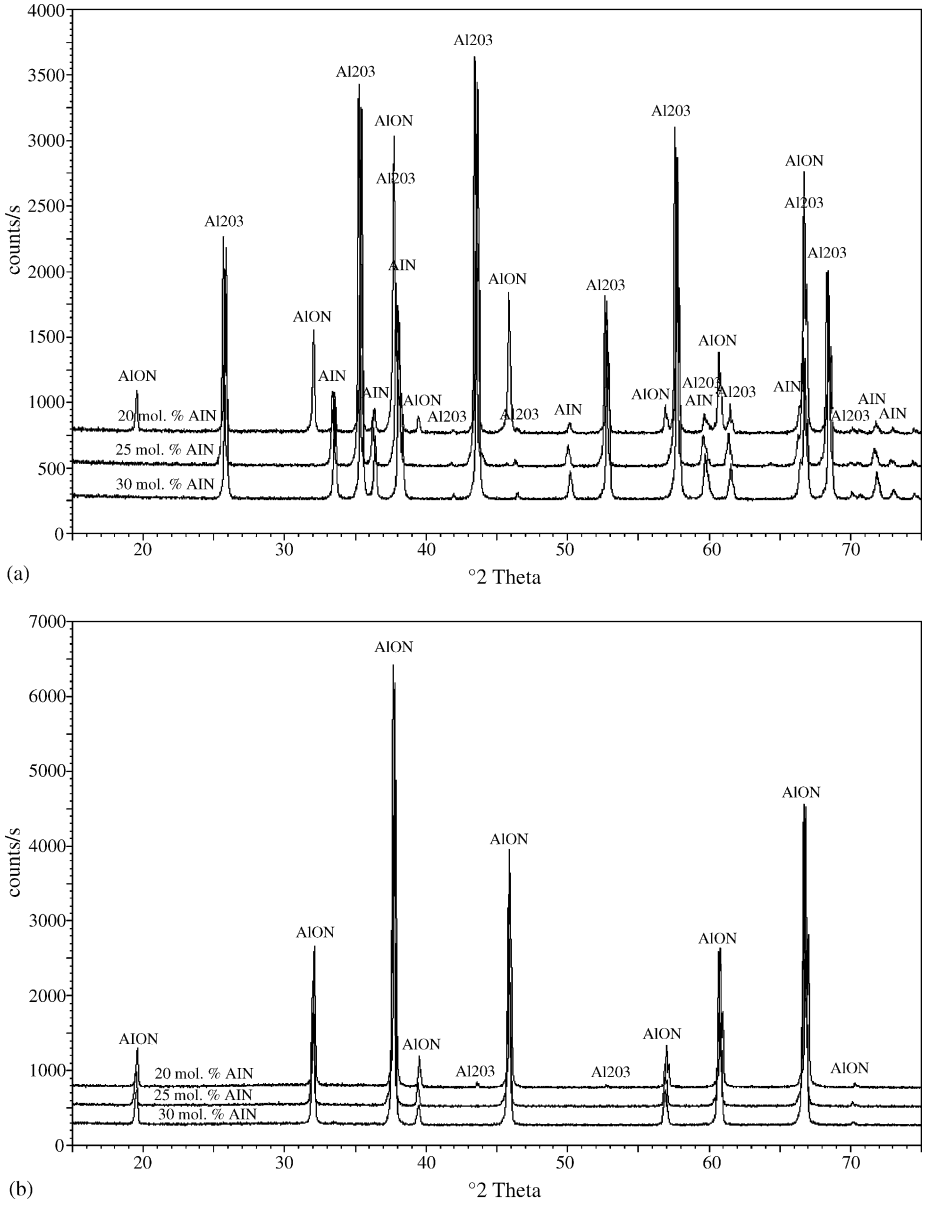

Fig. 2. X-ray patterns after reaction sintering Al_2O_3 with 20, 25, or 30 wt.% AlN at: (a) 1650 °C; or (b) 1850 °C for 2 h; and (c) comparison of Al_2O_3-25 mol% AlN at both temperatures.

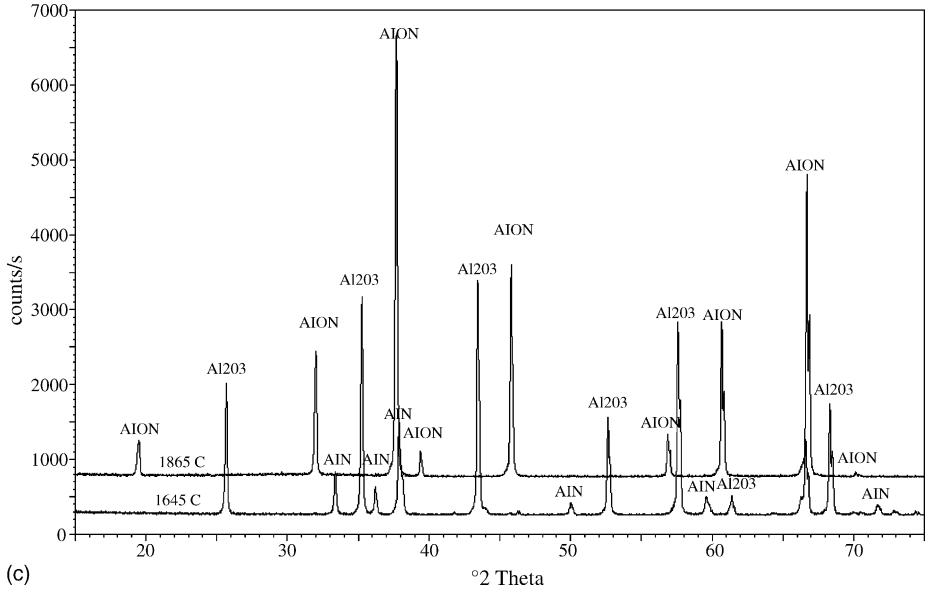

Fig. 2. (*Continued*).

stability regime (below 1640 °C) and then allow the expansion associated with the

$$\left(\frac{4-x}{3}\right) Al_2O_3 + xAlN \rightarrow Al_{(8+x)/3}V_{Al(1-x/3)}O_{4-x}N_x \quad (2)$$

phase change to decrease porosity. The volume expansion varies between 4.8 and 6.0 vol.% (≈1.6–2.0 linear %). Fig. 2 shows X-ray diffraction patterns after sintering at 1645 °C for 2 h in nitrogen. All three compositions were greater than 97% of theoretical after sintering at 1645 °C. The eutectoid composition is between 25 and 30 mol% AlN.[6–10] X-ray diffraction patterns confirm that after heating to 1865 °C for 2 h all of the Al_2O_3 and AlN converted to AlON. Fig. 3 shows the conversion occurring primarily between 1645 and 1765 °C regardless of the mole fraction of AlN. After heating to 1945 °C all three compositions were greater than 99.5% of theoretical density, but none of the compositions were translucent. Calcining the powders first to avoid the transformation still

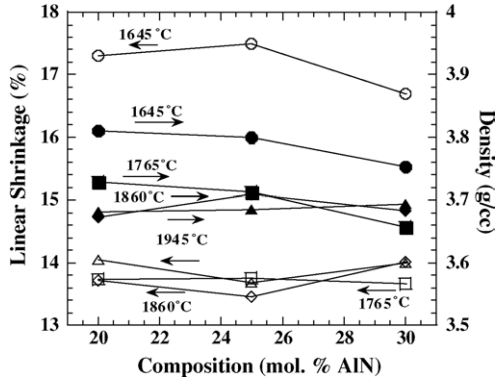

Fig. 3. Linear shrinkage and density of reaction sintered AlON at temperatures ranging from 1645 to 1945 °C as a function of AlN in the starting Al_2O_3/AlN powder.

permitted high density but did not make the samples transparent. Sintering with small additions of Mg^{2+} (MgO) and Y^{3+} (Y_2O_3 or YF_3) promoted sintering but parts were still opaque in spite of having densities near theoretical. Si^{4+} (Si_3N_4) and Nb^{5+} (Nb_2O_5) additions slowed down the sintering kinetics.

X-ray diffraction showed that zeta alumina was easily prepared by reaction sintering, as illustrated in Fig. 4. The advantage of the lower reaction temperature (900 °C rather than 1500 °C) was the higher surface area of the as-reacted powder. The surface area of the $LiAl_5O_8$ powder after calcining at 900 °C was similar to that of the alumina, at 7.6 m^2/g. The hypothesis was that $LiAl_5O_8$ would remain until it melted at 1915 °C and that after permitting particle rearrangement, it would allow the formation of AlON with the concurrent volatilization of lithia as:

$$\left(\frac{8-2x}{15}\right) LiAl_5O_8 + xAlN \rightarrow Al_{(8+x)/3}V_{Al((1-x)/3)}O_{4-x}N_x + \left(\frac{4-x}{15}\right) Li_2O \uparrow \quad (3)$$

The substitution of $LiAl_5O_8$ for Al_2O_3 on a constant Al molar basis therefore was used to assess the advantages of this approach for sintering AlON at an AlN content of 30 mol%. Zeta alumina additions promoted the formation of AlON by 1645 °C, with higher lithium promoting more transformation as shown by the X-ray diffraction patterns in Fig. 5. This reactive sintering approach slowed down the densification kinetics, as can be clearly observed by the density data in Fig. 6. The expected weight loss, based on Eq. (3), ranged from 0 to 3.5 wt.% for compositions containing between 0 and 64 wt.% $LiAl_5O_8$, respectively (Fig. 7). After sintering at 1945 °C for 2 h, the actual weight loss ranged between 0.32 and 1.3 wt.%, being lower than expected. X-ray diffraction showed only the AlON phase for all five compositions,

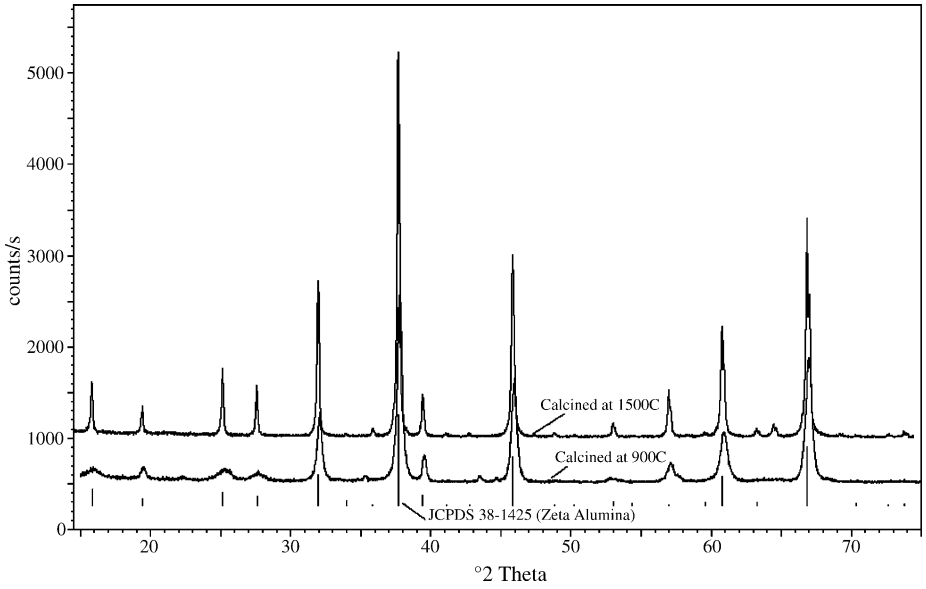

Fig. 4. Comparison of zeta alumina reacted at 900 or 1500 °C for 2 h.

but the highest $LiAl_5O_8$ sample bloated, as further evidence that all of the lithia was not fully removed from the sample. The remaining four compositions had densities between 3.67 and 3.68 g/cm^3, consistent with the XRD patterns. Compositions initially containing either 4 or 16 wt.% $LiAl_5O_8$ were translucent. Hardness increased with increasing N content in the AlON, but was independent of the amount of $LiAl_5O_8$ added to the starting powder and grain size, as shown by the data in Table 1. Annealing at 2000 °C for 15 h further increased the grain size and improved the light transmittance as shown in Fig. 8.

The effect of grain size on light transmittance was assessed by varying the annealing time and both the $LiAl_5O_8$ content and the Al_2O_3/AlN molar ratio. Light transmittance increased with increasing $LiAl_5O_8$ content and decreasing AlN content, as well as for increased annealing time, as shown by the samples in Fig. 9. Grain growth is enhanced by lithium aluminate content, increased O in the AlON, and sintering conditions (exponential with temperature and parabolic with time at temperature). Fig. 10 shows the effect of $LiAl_5O_8$ content on grain size. Table 2 gives data for AlON (20 mol% AlN) sintered with 22 wt.% $LiAl_5O_8$ in the starting powder,

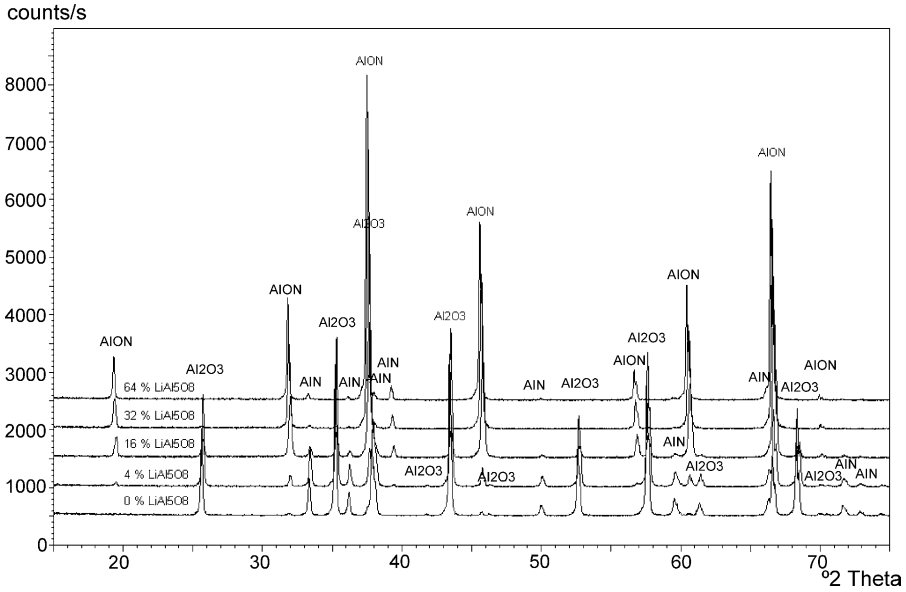

Fig. 5. Comparison of XRD patterns for reaction-sintered AlON (30 mol% AlN) compositions without zeta alumina and with increasing $LiAl_5O_8$ additions after sintering at 1645 °C for 2 h. Note how zeta alumina stabilizes the AlON phase at low temperatures.

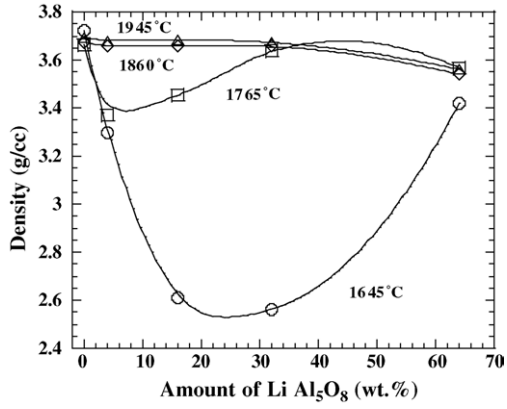

Fig. 6. Density as a function of $LiAl_5O_8$ added in AlON (Al_2O_3-30 mol% AlN) reaction-sintered compositions. Note that zeta alumina additions hinder sinterability.

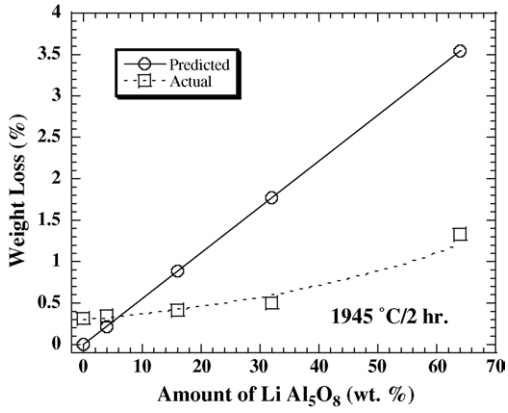

Fig. 7. Predicted and measured weight loss in AlON samples sintered with $LiAl_5O_8$ additions ranging between 0 and 64 wt.%.

showing the effect of temperature and annealing time on grain size. When the grain size becomes coarse, as was the case for the long annealing time at high temperature, the X-ray beam samples only a few grains, allowing texture to influence the

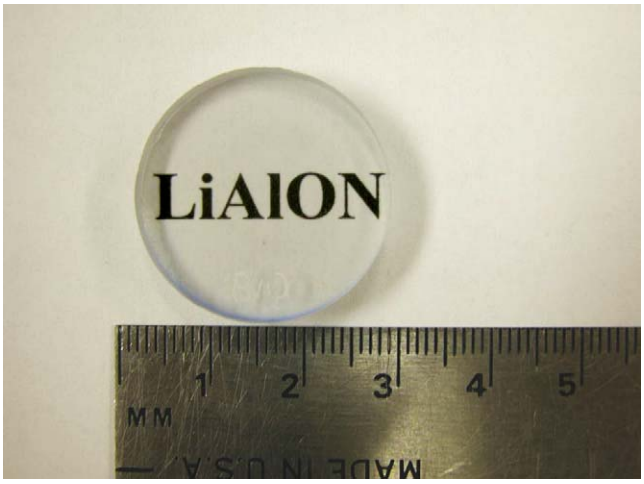

Fig. 8. LiAlON produced by pressureless sintering at 1900 °C for 2 h using a 30 mol% composition initially containing 16 wt.% $LiAl_5O_8$ and then HIPing at 2000 °C for 2 h. The sample is 6.2 mm thick.

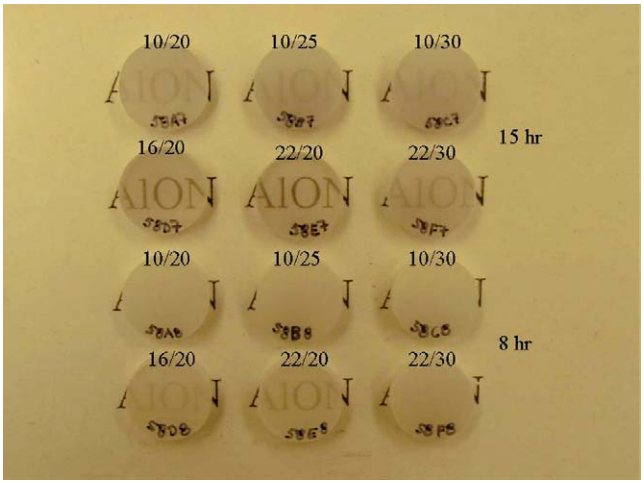

Fig. 9. AlON pressureless sintered at 2000 °C for either 8 or 15 h. The first number above each sample is the wt.% $LiAl_5O_8$ in the starting powder and the last number is the mol% AlN in the AlON solid solution.

Table 1
Effect of $LiAl_5O_8$ additions on hardness

$LiAl_5O_8$ (wt.%)	AlN (mol%)	Sintering temperature (°C)	Conditions time (h)	Density (g/cm^3)	HV1 hardness (GPa)
0	20	1945	2	3.670	15.9 ± 0.8
0	20	2000	2	3.670	15.4 ± 0.5
0	20	2000	15	3.659	15.6 ± 0.5
0	30	1945	2	3.678	15.7 ± 0.8
0	30	2000	2	3.690	16.6 ± 0.6
0	30	2000	15	3.691	16.4 ± 0.3
0	30	2000	30	3.659	16.5 ± 0.4
4	30	1945	2	3.686	16.5 ± 0.4
4	30	2000	2	3.688	16.1 ± 0.2
4	30	2000	15	3.688	16.9 ± 1.1
4	30	2000	30	3.679	17.0 ± 0.7
16	30	1945	2	3.683	16.4 ± 0.7
16	30	2000	2	3.686	16.7 ± 0.3
16	30	2000	15	3.687	16.5 ± 0.6
16	30	2000	30	3.670	16.4 ± 0.6

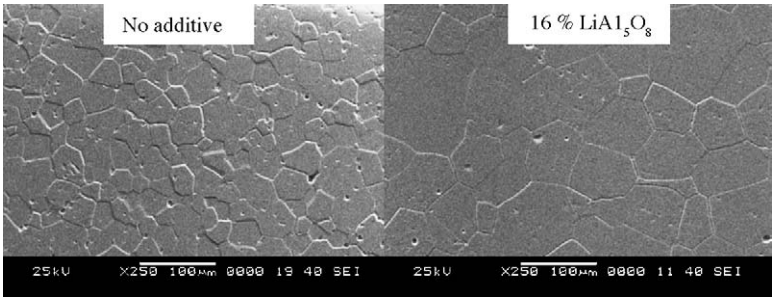

Fig. 10. Polished and etched AlON cross-sections for 30 mol% AlN samples sintered at 2000 °C for 15 h with and without $LiAl_5O_8$.

diffraction patterns, as shown in Fig. 11. If the sample is ground into powder then the peak intensities appear similar to the other samples. There was no effect of grain size on hardness, due to the fracture mode, which shows a considerable fraction of transgranular fracture (see Fig. 12). The higher temperatures and longer annealing times increase the density slightly, as shown by the data in Table 2.

Finishing was evaluated for the samples in Table 2, which had similar densities (all greater than 98.5% of theoretical and most greater than 99.5%) and hardness values. Differences

Table 2
Grain size and surface roughness for LiAlON (20 mol% AlN) made starting with 22 wt.% $LiAl_5O_8$

Sintering temperature (°C)	Conditions time (h)	Density (g/cm^3)	Grain size (μm)	Surface roughness[a]					
				DMG[b]		MRF[c]		Lap[d]	
				p–v (μm)	rms (nm)	p–v (μm)	rms (nm)	Time (h)	rms (nm)
1750	2	3.616 ± 0.001	12 ± 1.5	8.8 ± 1.0	536 ± 34	1.0 ± 0.3	54 ± 16	4	9 ± 2[e1]
1800	2	3.647 ± 0.001	30 ± 3	10 ± 2	662 ± 53	1.5 ± 0.5	76 ± 25	2	15 ± 1[e2]
1900	2	3.657 ± 0.001	68 ± 15	4.2 ± 0.7	86 ± 24	0.8 ± 0.3	87 ± 28	1	19 ± 5[e2]
2000	2	3.659 ± 0.003	86 ± 12	8.4 ± 2.0	201 ± 82	3.4 ± 0.7	165 ± 50	2	22 ± 52[e3]
2000	15	3.663 ± 0.001	470 ± 89	5.2 ± 1.9	140 ± 17	0.7 ± 0.2	109 ± 26	1	11 ± 7[e4]

[a] Peak-to-valley (p–v) and root mean square (rms) surface finish after finishing.
[b] After finishing with deterministic microgrinding.[22]
[c] After finishing with DMG followed by magnetorheological finishing.[23]
[d] After finishing with DMG followed by MRF and lapping with bound abrasives.[24]
[e] Sampling area: 1/0.175 × 0.132 mm^2; 2/0.349 × 0.262 mm^2; 3/0.890 × 0.668 mm^2; 4/2.11 × 1.58 mm^2.

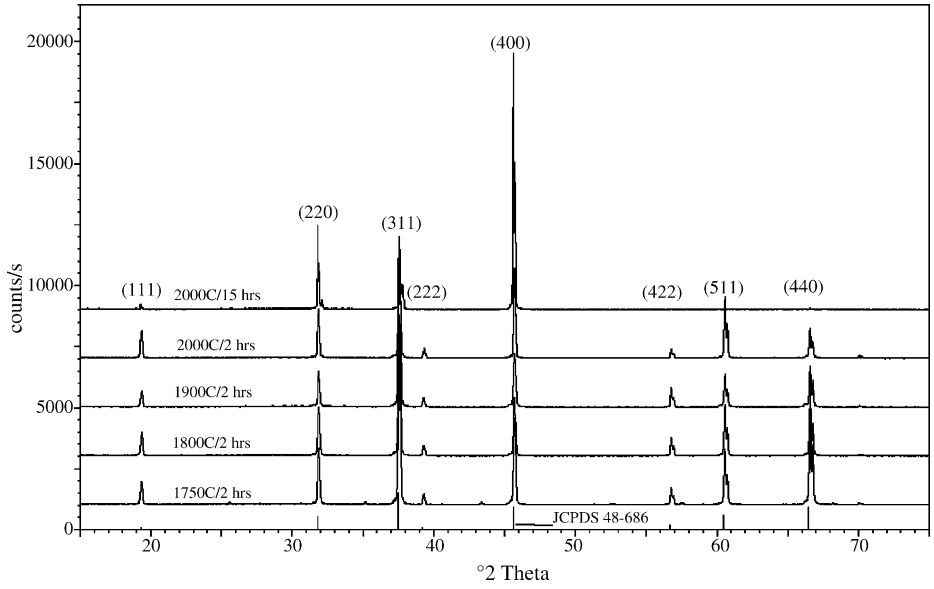

Fig. 11. X-ray diffraction patterns for AlON (20 mol% AlN) sintered with 22 wt.% $LiAl_5O_8$. Note trace of Al_2O_3 remaining at 1750 °C and texturing due to large grain size (see Table 2) when annealed at 2000 °C for 15 h.

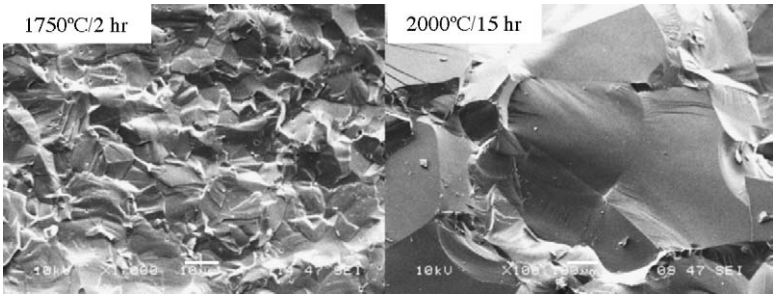

Fig. 12. Fracture surfaces of AlON (20 mol% AlN) sintered with 22 wt.% $LiAl_5O_8$ at 1750 °C/2 h or 2000 °C/15 h. Markers are 10 μm (left) and 100 μm (right).

were seen in the grindability of the fine-grained samples compared to the coarse-grained ones. Lower DMG in-feed rates (and consequently longer processing times) were required for the two fine-grained samples (12 and 30 μm), and it was not possible to reduce p–v and root mean square (rms) surface roughness below 9 and ∼0.5 μm, respectively. The larger grained samples (68, 86, and 470 μm) were more easily processed at higher in-feed rates (shorter processing times) to surface roughness levels of between 2.5–6.4 μm (p–v) and 0.075–0.123 μm (rms), respectively. All DMG surfaces were subjected to MRF without any pre-polishing.

After 2–3 h of polishing with MRF, it is estimated that from 4 to 6 μm of material were removed from all sample surfaces. Table 2 gives the initial (after DMG) and final (after MRF) surface roughness levels achieved. The p–v roughness levels for the two fine-grained samples (12 and 30 μm) were reduced by a factor of ten, but numerous pits were still present. Two of the larger grained samples (68 and 470 μm) were seen to behave in a similar fashion, but with less pitting observed in the processed surfaces. The sample with grain size of 86 μm was anomalous, in that the p–v could not be reduced below 3.4 μm, even after 3.5 h of processing and the removal of ∼7 μm of material.

With MRF processing directly after DMG, it was not possible to reduce rms roughness levels below 50–60 nm with many hours of polishing. Surface texture in the form of "orange peel" was visible to the eye on all samples. Polishing with epoxy-bound abrasives on flat "pin" laps was subsequently employed and, after one to four additional hours, rms roughness levels were further reduced to between ∼10 and ∼20 nm for all samples. The smallest grain size sample required a longer polishing time than the larger grain size samples.

An AlON (20 mol% AlN) sintered at 1800 °C to closed porosity with 22 wt.% $LiAl_5O_8$ in the powder was HIPed at 2000 °C in N_2 for 2 h at 207 MPa pressure. The density increased from 3.647 to 3.682 g/cm^3 while the grain size increased from 30 ± 3 to 78 ± 18 μm. It took 2.5 h to polish the HIPed part to a rms of 24 ± 7 nm using bound abrasives. Fig. 13 shows transmittance in the near-IR region comparing this 6.2 mm thick sample to a commercially available sample nearly three times as thick. Despite the thickness difference, it is evident that the transmission of the samples prepared experimentally are inferior to those produced commercially when ground using the same procedure. While the transmission in the IR and visible regions was not as high as desired, the samples made with lithium aluminate were much improved over samples made without this additive.

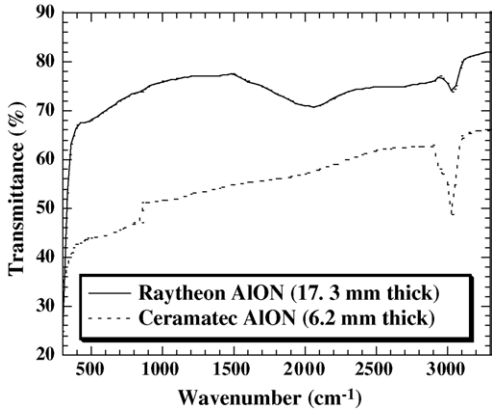

Fig. 13. Transmittance for a commercial (Raytheon) AlON compared to AlON prepared by pressureless sintering AlON (20 mol% AlON) sintered with 22 wt.% $LiAl_5O_8$ at 1800 °C and then HIPed in N_2 at 2000 °C for 2 h (Ceramatec) for wavelengths ranging between 3 and 33 μm.

4. Discussion

Bandyopadhyay et al.[25] showed that nitrogen diffusion was rate limiting when reaction sintering AlON and that complete conversion did not occur with their starting materials until temperatures exceeded 1800 °C, consistent with the results shown in Fig. 2. The volume expansion related to the conversion of Al_2O_3 and AlN to AlON is problematic for large components, such as armor tiles, if densification occurs first, since creep rates need to exceed the expansion rates in order to avoid cracking. A better solution is to allow conversion during reaction sintering with $LiAl_5O_8$ additions, while the material is still porous and has a lower modulus. The formation of large armor tiles is possible using this approach. Zeta alumina is a cubic spinel at low temperatures identical in structure to Al_2O_3 with 11.4% AlN dissolved in it.[1] Schwetz et al.[26] showed that small Li_2O additions stabilize γ-AlON formation in early sintering work with AlN. In the present work, when LiF or Li_2O was substituted for $LiAl_5O_8$, at the

same Li/Al ratio in the reaction sintering process, low temperature stabilization did not occur. Similarly, these additives did not result in AlON with good light transmittance, despite allowing AlON to densify to near theoretical density.

Lejus and Collongues[27] showed that cubic $LiAl_5O_8$ undergoes an order-disorder phase transformation at 1290 °C from the ordered low-temperature phase (space group $P4_332$ with $a = 7.908$ Å) to the disordered high-temperature phase (space group $Fd3m$ with $a = 7.925$ Å). Willems et al.[7] report lattice parameters of 7.945 and 7.932 Å for the oxygen-rich phase boundary of γ-AlON (space group $Fd3m$) at 1650 and 1850 °C, respectively. Kriens et al.[28] reported a $Li_2Al_4O_7$ spinel with this same cubic structure and lattice parameter (space group $F3dm$ (227) with $a = 7.910$ Å) requiring oxygen vacancies for charge neutrality. Al^{3+} occupy both the octahedral and the tetrahedral sites in γ-AlON. Li^+ cations occupy octahedral sites in ordered $LiAl_5O_8$ and nearly 50% more octahedral sites than tetrahedral sites in $Li_2Al_4O_7$. It appears likely that Li^+ can substitute for Al^{3+} in the γ-AlON spinel structure to make a γ-LiAlON spinel, filling both octahedral and tetrahedral sites. Charge neutrality requirements allowing Li^+ substitution for Al^{3+} into γ-AlON would result in reduced Al vacancy formation or introduction of AlN into disordered $LiAl_5O_8$ would require vacancy formation on the anion sublattice. The cation vacancy (V^c) electroneutrality requirements is given by:

$$(Li_yAl_{(1-y)})_{3-z}V_z^cO_{4-x}N_x \quad (4)$$

where x and y range between 0 and 1 while $z = (1 - x - 6y)/(3 - 2y)$. For anion vacancy ($V^a$) formation electroneutrality requires that:

$$(Li_yAl_{(1-y)})_3(O_{4-x}N_x)_{1-z}V_z^a \quad (5)$$

where x and y range between 0 and 1 while $z = (9 - 8y)/(8 + x)$. Of course, both cation and anion vacancies are possible simultaneously in analogy to the $MgAl_2O_4$ system.[29] Fig. 14 shows the calculated vacancy formation based on Eqs. (4) and (5) indicating that cation vacancies dominate at low levels of $LiAl_5O_8$ and that anion vacancies are required as most of the Al_2O_3 is replaced by $LiAl_5O_8$ in the reaction sintering process. Since anion vacancies speed up the sintering kinetics of $MgAl_2O_4$,[30] it is not surprising that at 1645 °C that sintering is enhanced for the 64 wt.% $LiAl_5O_8$ addition (anion vacancies are predicted from Fig. 14 for this 30 mol% AlN composition) compared to the 16 or 32 wt.% $LiAl_5O_8$ compositions where cation vacancies dominate (see Fig. 6). There is no or little LiAlON formation at 0 and 4 wt.% zeta alumina additions so that sintering is not controlled by vacancy formation for these compositions. Structural parameter measurements combined with careful inductively coupled plasma (ICP) chemical analysis are required to give further insight into vacancy formation of γ-LiAlON spinels. Weight loss measurements and high-temperature bloating of samples with high starting amounts of zeta alumina suggest that all of the lithia did not leave the samples.

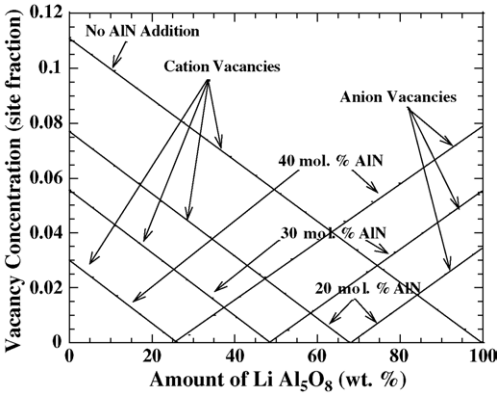

Fig. 14. Calculated cation or anion vacancy formation in LiAlON (30 mol% AlN/70 mol% Al_2O_3) as a function of lithium cation addition.

$LiAl_5O_8$ additions promote grain growth indicating that once the reaction sintering process is completed that vacancy formation may enhance diffusion. The role of zeta alumina is clearly defined in Fig. 10 and Table 2, where it is obvious that increasing amounts of zeta alumina result in larger grain size. At first glance it is easy to arrive at the conclusion that grains are scattering light. Assume, however, that there are pores with an average size of 0.5 μm, in the same range as the wavelength of light and that there is, on average, one pore attached (along a grain boundary) to each grain. Then the total number of pores (i.e., light scattering sites) in a cubic centimeter of a sample with an average grain size of 10 μm would be one trillion. The volume of these pores would be 0.007%, or the part could still be 99.993% of theoretical density. If in this hypothetical situation, the grain size grows by an order of magnitude and the porosity remains constant, then the scattering of light decreases for two reasons: (1) the number of pores decreases, due to pore coalescence, by a factor of one thousand, which decreases the scattering coefficient by decreasing the number of scattering centers; and (2) the pore size grows to 5 μm, which is further away from the critical size for scattering light and thereby decreases the scattering coefficient.[31] While this simple logic certainly has flaws in it, such as the neglect of capillary pressure causing pores to shrink or elimination of voids by diffusion to free surfaces, it shows how grain growth could lead to higher in-line light transmission.

It must be reiterated that large grain size is not critical for attaining transparent ceramics. Gazza and Dutta[32] made transparent $MgAl_2O_4$ or $LiAl_5O_8$ with a 1 μm grain size by vacuum hot pressing at 10^{-8} bar. The low pressure removed gases that would normally have been trapped within pores, limiting porosity. The critical consideration is the pressure inside the pore at the onset of pore closure, since the pressure inside a closed pore must be balanced by the driving force for sintering. Gazza or Dutta[32] were able to minimize the pressure inside the pores at the onset of closed porosity by using a high vacuum and allowing enough time for diffusion of any remaining gases from the pore structure. The

improvement in transparency with HIPing is an alternative method for closing pores, but requires higher temperatures due to the grain size dependency upon creep rate. It is now apparent that fine-grained materials can be made transparent if excellent particle packing allows the elimination of voids that scatter light.[33,34]

While it is well known that lithia additions can influence the grain growth in alumina-based ceramics[35,36] it is not as apparent why $LiAl_5O_8$ was more effective than Li_2O or LiF. One possibility is that zeta alumina allows a more effective means of distributing the lithia.[37] It is more likely, however, that the high-temperature disordered FCC spinel structure of zeta alumina, which matches that of γ-AlON, speeds up the reaction kinetics. Further work is required to look at the thermodynamic stability of LiAlON.

A major challenge with AlON is the influence of sintering atmosphere upon stoichiometry. Willems et al.[7] showed that AlON stoichiometry is dependent on both the partial pressures of oxygen and nitrogen. Higher pressures of N_2 increase the nitrogen content. Using lattice parameter measurements and the calibration curve proposed by Willems et al.[7] it was possible to show a shift from 20 mol% AlN to 23 mol% AlN during reactive sintering in nitrogen. Correspondingly, the 30 mol% AlN AlON increased in nitrogen content to 32% based on lattice parameters. Patel et al.[38] saw similar shifts when sintering at high temperatures in nitrogen.

Hardness is somewhat dependent on nitrogen content in the AlON increasing for a material made with 10 wt.% $LiAl_5O_8$ from 15.9 ± 0.4 GPa at 20 mol% AlN to 17.0 ± 0.5 GPa at 25 mol% AlN and 16.9 ± 0.7 GPa for 30 mol%. These results are consistent with the values reported in Table 1 as well as with literature data. The hardness is in line with expectation. Willems et al.[39] measured a Vickers hardness for AlON made with 27 and 33 mol% AlN of 16.1 ± 0.7 and 17.7 ± 1.1 GPa, respectively. Vickers hardness values of 14–16 GPa were reported over a wide range of stoichiometries.[40] Knoop hardness values of 13.8 ± 0.3[41] for a 2 kg load and higher values (16.5–19.5 GPa) for low loads[5] are prevalent in the literature.

The initial premise that a transient liquid phase formation would be created by the addition of zeta alumina proved to be invalid, as zeta alumina promoted the early formation of AlON and was no longer identified by X-ray diffraction at 1640 °C. Furthermore, the premise that fine-grained materials would be easier to finish due to lower grain pullout also appears to be false. This may be due to the mixed fracture mode. Transgranular fracture makes grain pullout more difficult. Sintered SiC is an example of a material that fractures predominately transgranularly and shows little effect of grain size on hardness or surface finish. Fig. 12 and the hardness data in Table 1 show that this same tendency exists in AlON materials. It is recognized that the finishing work done was very preliminary and more work is required before firm conclusions can be made in this regard.

Since the pioneering work of McCauley and Corbin[4] on reaction sintering there have been many attempts to use this approach. Most have found that it is easy to reach high density, but it is difficult to make the materials transparent.[42,43] The partial replacement of Al_2O_3 with $LiAl_5O_8$ in the reaction sintering process solves this dilemma. While it is very apparent from Fig. 13 that this experimental material lags far behind commercially available AlON it is believed that with improved processing defects can be eliminated in the green state and higher in-line transmission obtained. However, unless the cost of finishing can be substantially reduced, the use of inexpensive raw materials alone does not represent a substantial cost savings in the production of pressureless sintered AlON.

5. Conclusions

Al_2O_3, $LiAl_5O_8$, and AlN could be reaction sintered to give approximately 65% in-line transmission in the visible region for 6.2 mm thick LiAlON. The replacement of $LiAl_5O_8$ for Al_2O_3 did not enhance sintering, as early LiAlON formation hindered sintering. The attainment of densities approaching theoretical was possible with or without zeta alumina additions, but the addition of $LiAl_5O_8$ in the range of 10–20 wt.% of the starting composition resulted in a distinct difference in light transmission. Weight loss measurements combined with X-ray diffraction patterns suggest that most of the lithia remains within the spinel structure. This suggests that γ-LiAlON structures are stable at elevated temperatures. This deserves more attention and careful structure parameter measurements.

The main role of $LiAl_5O_8$, however, appears to be in promoting the growth of equiaxed LiAlON grains, which are believed to reduce the number of scattering sites by pore coalescence. Samples with zeta alumina additions were the only compositions that were made transparent using comparative processes of a variety of sintering aids and compositions. It was possible to make transparent LiAlON by sintering at 1800 °C to reach closed porosity and then HIPing at 2000 °C for 2 h in 207 MPa N_2. The grain size was 80 ± 14 μm. Alternatively, pressureless sintering, without HIPing, resulted in transparency if the parts were annealed at 2000 °C for 10–15 h to grow grains. Hardness for all samples was similar to commercially available AlON, which is on the order of 17 GPa when measured with a 1-kg load Vickers indent. The in-line transmission was inferior to commercially available AlON and improved processing would be needed to eliminate defects in the green state.

Grinding and polishing of LiAlON with grain sizes ranging between 10 and 500 μm showed no evidence that finer-grain size resulted in better surface finish or shorter processing times. While reaction sintering represents a substantial savings in raw materials costs, major savings for transparent AlON is only possible if finishing costs are substantially reduced.

Acknowledgements

This work was partially funded by the Idaho Nuclear Engineering and Environmental Laboratory (INEEL) under contract no. 12664. Discussions with Dr. Tom Lillo and Dr. Henry Chu of INEEL were very helpful. The authors acknowledge Frank Mrakovcic, Leslie Gregg, Irina Kozhinova, Anne Marino, and Henry Romanofsky, all of the University of Rochester, for grinding and polishing samples, and for making transmission measurements.

References

1. Long, G. and Foster, L. M., Crystal phases in the system Al_2O_3-AlN. *J. Am. Ceram. Soc.*, 1961, **44**(6), 255.
2. McCauley, J. W., A simple model for aluminum oxynitride spinels. *J. Am. Ceram. Soc.*, 1978, **61**(7/8), 372.
3. Lejus, A., Formation at high temperature of nonstoichiometric spinels and of derived phases in several oxide systems based on alumina and in the system alumina-aluminum nitride. *Rev. Int. Hautes Temp. Refrac.*, 1964, **1**(1), 53.
4. McCauley, J. W. and Corbin, N. D., Phase relations and reaction sintering of transparent cubic aluminum oxynitride spinel (ALON). *J. Am. Ceram. Soc.*, 1979, **62**(9–10), 476.
5. Corbin, N. D., Aluminum oxynitride spinel: a review. *J. Eur. Ceram. Soc.*, 1989, **5**(3), 143.
6. Hillert, M. and Jonson, S., Thermodynamic calculation of the Al-N-O system. *Z. Metallkd.*, 1992, **83**(10), 714.
7. Willems, H. X., Hendrix, M. M. R. M., de With, G. and Metselaar, R., Thermodynamics of AlON II: phase relations. *J. Mater. Sci.*, 1992, **10**, 339.
8. Dumitrescu, L. and Sundman, B., A thermodynamic reassessment of the Si-Al-O-N system. *J. Eur. Ceram. Soc.*, 1995, **15**(3), 239.
9. Qui, C. and Metselaar, R., Phase relations in the aluminum carbide-aluminum nitride-aluminum oxide system. *J. Am. Ceram. Soc.*, 1997, **80**(8), 2013.
10. Nakao, W., Fukuyama, H. and Nagata, K., Thermodynamic stability of γ-aluminum oxynitride. *J. Electrochem. Soc.*, 2003, **150**(2), J1.
11. Willems, H. X., de With, G. and Metselaar, R., Thermodynamics of AlON III: stabilization of AlON with MgO. *J. Eur. Ceram. Soc.*, 1993, **12**(1), 43.
12. Granon, A., Goeuriot, P. and Thevenot, F., Aluminum magnesium oxynitride: a new transparent spinel ceramic. *J. Eur. Ceram. Soc.*, 1995, **15**(3), 249.
13. Hartnett, T. M., Bernstein, S. D., Maguire, E. A. and Tustison, R. W., Optical properties of ALON. *SPIE*, 1997, **3060**, 284.
14. Maguire, E. A., Rawson, F. K. and Tustison, R. W., Aluminum oxynitrides resistance to impact and erosion. *SPIE*, 1994, **2286**, 26.
15. Swab, J. J., LaSalvia, J. C., Gilde, G. A., Patel, P. J. and Motyka, M. J., Transparent armor ceramics: AlON and spinel. *Ceram. Eng. Sci. Proc.*, 1999, **20**, 79.
16. Hartnett, T. M., Gentilman, R. L. and Maguire, E. A., *Aluminum Oxynitride Having Improved Optical Characteristics and Method of Manufacture*. U.S. Patent 4,481,300 (6 November 1984).
17. Gentilman, R. L., Maguire, E. A. and Dolhert, L. E., *Transparent Aluminum Oxynitride and Method of Manufacture*. U.S. Patent 4,520,116 (28 May 1985).
18. Maguire, E. A., Hartnett, T. M., Gentilman, R. L., Method of producing aluminum oxynitride having improved optical characteristics. U.S. Patent 4,686,070 (11 August 11 1987).
19. Gentilman, R. L., Maguire, E. A. and Dolhert, L. E., *Transparent Aluminum Oxynitride and Method of Manufacture*. U.S. Patent 4,720,362 (19 January 1988).
20. Cook, L. P. and Plante, E. R., Phase diagram of the system lithia-alumina. *Ceram. Trans.*, 1992, **27**(3), 193.
21. Rhodes, W. H., Controlled transient solid second-phase sintering of yttria. *J. Am. Ceram. Soc.*, 1981, **64**(1), 13.
22. Lambropoulos, J. C., Gillman, B. E., Zhou, Y., Jacobs, S. D. and Stevens, H. J., Glass-ceramics: deterministic microgrinding, lapping, and polishing. *SPIE*, 1997, **3134**, 178.
23. Jacobs, S. D., Arrasmith, S. R., Kozhinova, I. A., Gregg, L. L., Shorey, A. B., Romanofsky, H. J. *et al.*, An overview of magnetorheological finishing (MRF) for precision optics. *Ceram. Trans.*, 1999, **102**, 185.
24. Gregg, L. L., Marino, A. E., Hayes, J. and Jacobs, S. D., Grain decoration in aluminum oxynitride (ALON) from polishing on bound abrasive laps. *SPIE*, 2004, **5810**, 47.
25. Bandyopadhyay, S., Rixecker, G., Aldinger, F., Pal, S., Mukherjee, K. and Maiti, H. S., Effect of reaction parameters on the γ-AlON formation from Al_2O_3 and AlN. *J. Am. Ceram. Soc.*, 2002, **85**(4), 1010.
26. Schwetz, K. A., Knoch, H. and Lipp, A., Sintering of aluminum nitride with low oxide addition. In *Progress in Nitrogen Ceramics*, ed. F. L. Riley. Martinus Nijhoff, Boston, 1983, pp. 245–252.
27. Lejus, A. M. and Collongues, R., The structure and properties of lithium aluminates. *Compt. Rend.*, 1962, **254**, 2005.
28. Kriens, M., Adiwidjaja, W., Guse, W., Klaska, K. H., Lathe, C. and Saalfeld, H., The crystal structures of $LiAl_5O_8$ and $Li_2Al_4O_7$. *Neus Jahrbuch fuer Mineralogie*, 1996, **8**, 344.
29. Kume, T., Kuwabara, T., Sakurada, O., Hashiba, M., Nurishi, Y., Requena, J. *et al.*, Ionic transport to produce diverse morphologies in $MgAl_2O_4$ formations started from powders of varied physical nature. In *Ceramic Microstructure: Control at the Atomic Level*, ed. A. P. Tomsia and A. Glaeser. Plenum Press, New York, 1998, p. 577.
30. Ting, C. J. and Lu, H. Y., Defect reactions and the controlling mechanism in the sintering of magnesium aluminate spinel. *J. Am. Ceram. Soc.*, 1999, **82**(4), 841.
31. Tilley, R., *Colour and the Optical Properties of Materials*. Wiley, New York, 2000, p. 109.
32. Gazza, G. E. and Dutta, S. K., *Hot Pressing Ceramic Oxides to Transparency by Heating in Isothermal Increments*. U.S. Patent 3,767,745 (23 October 1973).
33. Godlinski, D., Kuntz, M. and Grathwohl, G., Transparent alumina with submicrometer grains by float packing and sintering. *J. Am. Ceram. Soc.*, 2002, **85**(10), 2449.
34. Apetz, R. and van Bruggen, M. P. B., Transparent alumina: a light scattering model. *J. Am. Ceram. Soc.*, 2003, **86**(3), 480.
35. Sumita, S. and Bowen, H. K., Effects of foreign oxides on grain growth and densification of sintered alumina. *Ceram. Trans.*, 1988, **1**, 840.
36. Jatkar, A. D., Cutler, I. B. and Gordon, R. S., Conversion catalysis and microstructure control in the sintering of lithia-stabilized β″-alumina. In *Ceramic Microstructures*, ed. R. M. Fulrath and J. A. Pask. Westview Press, Boulder, Co., 1977, p. 414.
37. Youngblood, G. E., Virkar, A. V., Cannon, W. R. and Gordon, R. S., Sintering processes and heat transfer schedules for conductive, lithia-stabilized β″-alumina. *Am. Ceram. Soc. Bull.*, 1977, **56**(2), 206.
38. Patel, P. J., Gilde, G. and McCauley, J. W., The role of gas pressure in transient liquid phase sintering of aluminum oxynitride (AlON). *Ceram. Eng. Sci. Proc.*, 2003, **24**, 425.
39. Willems, H. X., Van Hal, P. F., de With, G. and Metselaar, R., Mechanical properties of γ-aluminum oxynitride. *J. Mater. Sci.*, 1993, **28**, 6185.
40. Yamashita, H. and Yamaguchi, A., Preparation and properties of aluminum oxynitride. *J. Ceram. Soc. Jpn.*, 2001, **109**(4), 310–314.

41. Patel, P. J., Glide, G. A., Dehmer, P. G. and McCauley, J. W., Transparent ceramics for armor and EM window application. *SPIE Proc.*, 2000, **4102**, 1.
42. Chen, C. F., Savrun, E. and Ramirez, A. F., Densification and phase transformation of pressureless reactive sintered aluminum oxynitride (AlON) ceramics. *Mater. Sci. Monogr.*, 1991, **66B**, 1295.
43. Xidong, W., Fuming, W. and Wenchao, L., Synthesis, microstructures and properties of γ-aluminum oxynitride. *Mater. Sci. Eng.*, 2003, **A342**, 245.